JACS
JOURNAL OF THE AMERICAN CHEMICAL SOCIETY
pubs.acs.org/JACS
Communication

Hydrazonyl Sultones as Stable Tautomers of Highly Reactive Nitrile Imines for Fast Bioorthogonal Ligation Reaction

Ming Fang, Gangam Srikanth Kumar, Stefano Racioppi, Heyang Zhang, Johnathan D. Rabb, Eva Zurek, and Qing Lin*

Cite This: J. Am. Chem. Soc. 2023, 145, 9959–9964
Read Online

ABSTRACT: Here we report the design and synthesis of a new class of bioorthogonal reagents called hydrazonyl sultones (HS) that serve as stable tautomers of highly reactive nitrile imines (NI). Compared to the photogenerated NI, HS display a broad range of aqueous stability and tunable reactivity in a 1,3-dipolar cycloaddition reaction, depending on substituents, sultone ring structure, and solvent conditions. DFT calculations have provided vital insights into the HS → NI tautomerism, including a base-mediated anionic tautomerization pathway and a small activation barrier. Comparative kinetic analysis of tetrazole vs HS-mediated cycloadditions reveals that a tiny fraction of the reactive NI (~15 ppm) is present in the tautomeric mixture, underpinning the extraordinary stability of the six-membered HS. We further demonstrate the utilities of HS in selective modification of bicyclo[6.1.0]non-4-yn-9-ylmethanol (BCN)-lysine-containing nanobodies in phosphate buffered saline and fluorescent labeling of a BCN-lysine-encoded transmembrane glucagon receptor on live cells.

Bioorthogonal ligation reactions provide a robust set of chemistry-based precision tools to visualize the dynamic distribution of biomolecules in native cellular environment and to deliver cytotoxins selectively to specific tumor tissues.[1−3] A key endeavor in bioorthogonal reaction development is to harness biocompatible reactive intermediates for fast, chemoselective ligation reactions in complex systems, including living animals. Because of their inherently high reactivity, the reactive intermediates are frequently generated *in situ* with the help of a light[4,5] or redox trigger[6] such as a chemical, a photocatalyst, and an enzyme. These biocompatible photo/redox-activatable precursors include the photocaged DHTz,[7] 9,10-phenanthrenequinone (PQ),[8] diarylazirine,[9] diarylsydnone,[10] diaryltetrazole,[11] dihydrotetrazine (DHTz),[12−14] and 1,2-catechol[15,16] (Figure 1a,b). Because visible light has limited tissue penetration, photochemical precursors activatable by near-IR light have also been reported.[17,18] For oxidation-triggered reactions, it is extremely hard to confer a redox control without affecting the surrounding environment in a living system. Therefore, alternative strategies that permit autonomous access of reactive intermediates for potential systemic use in living animals are highly desirable.

The word tautomerism was coined by Laar in 1886 to describe dynamic equilibria among isomeric structures that differ in their positions of proton and double bonds. In particular, the ring−chain tautomerism,[19] in which one of the tautomers is in the cyclic form, is crucial in biological chemistry. More recently, less stable minor tautomers but with high reactivity have been exploited in the concerted cycloaddition reactions.[20,21] In harnessing reactive intermediates for bioorthogonal reactions, here we report the design and synthesis of hydrazonyl sultones (Figure 1c) as stable tautomers of the highly reactive nitrile imines, the characterization of their stability in aqueous media and their selective

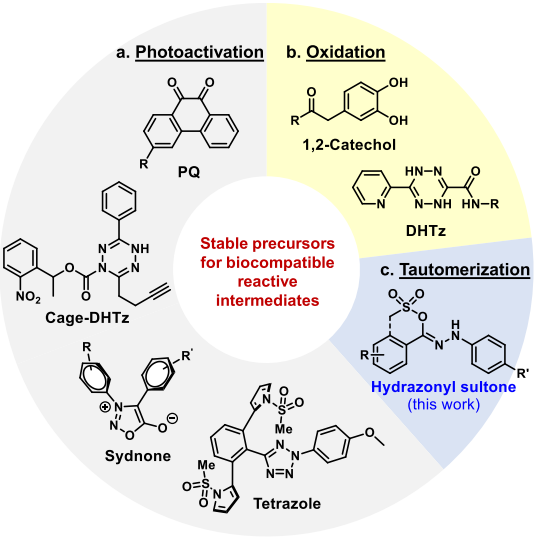

Figure 1. Donut chart showing three strategies for accessing biocompatible reactive intermediates for bioorthogonal ligation reactions: (a) photoactivation, (b) oxidation, and (c) tautomerization, with representative precursor structures.

reactivity toward bicyclo[6.1.0]non-4-yn-9-ylmethanol (BCN) in the 1,3-dipolar cycloaddition reaction, and the demon-

Received: November 20, 2022
Published: April 27, 2023

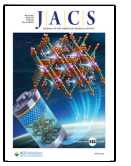

https://doi.org/10.1021/jacs.2c12325
J. Am. Chem. Soc. 2023, 145, 9959−9964

stration of their utility in bioorthogonal modification of proteins in solution and on live cells.

To identify a stable tautomeric form of the nitrile imine (NI), we noted in our earlier work that an *ortho*-carboxylic acid group on the C-aryl ring reacts readily with an *in situ* generated NI to form a stable hydrazonyl lactone;[22] however, the lactone failed to regenerate the reactive NI under all the conditions tested. Inspired by the successful deployment of a spirocyclization strategy in the design of cell-permeable rhodamine-based dyes,[23,24] we envisioned that a leaving group at the ortho position with a lower pK_a value of its conjugate acid might facilitate the ring rupture. Thus, a small panel of ring forms of NI carrying an ortho-leaving group with pK_a values ranging from 5.2 to −2.6 was prepared (Figure 2a), and their reactivity

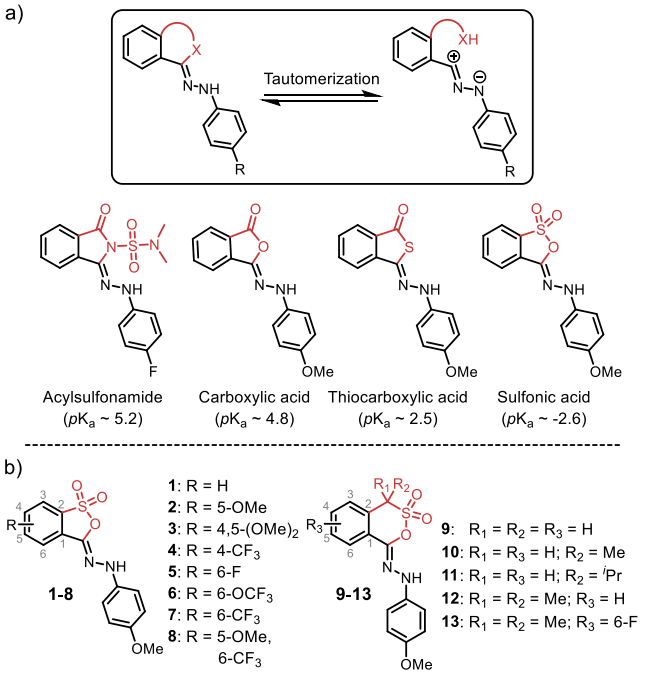

Figure 2. (a) Selecting an appropriate leaving group (highlighted in red) based on pK_a value of its conjugated acid for facile ring−chain tautomerization. (b) Structures of five-membered hydrazonyl sultones (**1**−**8**) and six-membered hydrazonyl sultones (**9**−**13**).

toward dimethyl fumarate was assessed (Table S1). To our delight, we found that the sultone ring appeared to release the NI tautomer and produced a fluorescent cycloadduct. We refer to this tautomeric structure as hydrazonyl sultone (HS) based on the combination of two essential functional groups. Encouraged by this result, we synthesized 12 additional HS from the corresponding sulfonic acid-containing tetrazoles via photogeneration of the NI followed by instantaneous nucleophilic addition with the *ortho*-sulfonic acid. Because ring size plays a crucial role in ring−chain tautomerization,[19] we prepared both five- and six-membered HS to interrogate a broad range of stability and reactivity (Figure 2b, Schemes S1−S7).

To investigate if tautomerism offers a stable NI precursor, we measured the HS stability in phosphate buffered saline (PBS)−acetonitrile (Table 1, Table S2, and Figure S1). The half-life of **HS-1** was determined to be 20.8 ± 0.1 min. Substitution at the C-phenyl ring had a modest effect, with **HS-2**, **-6**, and -7 showing 2−6 times longer half-life than **HS-1** (Table 1). The higher stability can be attributed to a higher

Table 1. Stability of Hydrazonyl Sultones 1−13 and Their Reactivity in the Cycloaddition Reaction with BCN

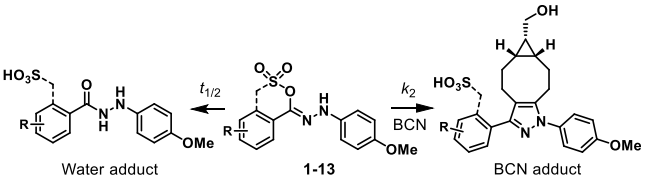

HS	$t_{1/2}$ (min)[a]	k_2 (M^{-1} s^{-1})[b]
1	20.8 ± 0.1	285 ± 10
2	64.0 ± 1.8	290 ± 10
3	12.2 ± 0.1	260 ± 4
4	10.9 ± 0.1	2690 ± 259
5	8.62 ± 0.17	4270 ± 183[c]
6	48.2 ± 0.4	2330 ± 148
7	114 ± 1	2005 ± 96
8	18.5 ± 0.3	3678 ± 343[c]
9	17.6 ± 0.2	89.5 ± 1.2
10	203 ± 2	18.3 ± 0.4
11	1460 ± 49	2.18 ± 0.01
12	>48 h[d]	<0.02
13	>48 h[d]	0.274 ± 0.003[e]

[a]Absorbance of a solution of 100 μM HS in 0.5 mL of PBS−ACN (1:1) at 353 nm was monitored by UV−vis. [b]Absorbance of a solution of 20 μM HS and 200 μM of BCN in 0.5 mL of PBS−ACN (1:1) at 353 nm was monitored by UV−vis. [c]100 μM BCN was used. [d]Hour unit is used. [e]2 mM BCN was used.

sulfonic acid pK_a value due to 5-OMe substitution[25] or the electronic repulsion against water addition by 6-OCF_3[26] and 6-CF_3 groups.[27] On the other hand, **HS-5** with fluorine at position-6 gave the shortest half-life (Table 1), presumably due to the generation of a highly electrophilic nitrile imine. In contrast, the six-membered HS displayed far greater stability, with $t_{1/2}$ exceeding 48 h for **HS-12** and **-13**. We attribute this extraordinary stability to a favorable ring size[19] and the torsional effect of the *gem*-dimethyl group.[28]

To probe if stable HS tautomers remain competent in the cycloaddition reactions, we incubated HS with BCN and monitored the product formation based on HS decay. HS showed a broad range of reactivity with the apparent second-order rate constants of 0.274 ± 0.003 M^{-1} s^{-1} for the most stable **HS-13** and 4270 ± 183 M^{-1} s^{-1} for the least stable **HS-5** (Table 1 and Figure S2). In general, five-membered HS gave faster reactions than six-membered HS. However, **HS-7** showed a long half-life ($t_{1/2}$ ≈ 2 h) and excellent reaction kinetics (k_2 ≈ 2000 M^{-1} s^{-1}), indicating a nonlinear relationship between stability and cycloaddition reactivity. Indeed, **HS-9** displayed similar stability to **HS-8** but more than 40 times slower reaction kinetics, suggesting other factors such as HOMO energies[29] of the NI may also contribute. For six-membered HS, the unusually high stability of **HS-12** was attenuated when fluorine was added to the ortho position as in **HS-13**, which gave slow but measurable kinetics (Table 1). Furthermore, incubation of HS with an equal molar BCN/glutathione mixture showed excellent selectivity for the cycloaddition (92−100%), as monitored by LC−MS, with a negligible amount of side products from GSH addition, HS hydrolysis, or dimerization (Table S3, Figure S3).

To gain a structural understanding of the HS stability−reactivity trend, we obtained the crystal structures of **HS-1**, **-9**, and **-12** (Figure 3, Tables S4−S6). We note that the C1−S1−

https://doi.org/10.1021/jacs.2c12325
J. Am. Chem. Soc. 2023, 145, 9959−9964

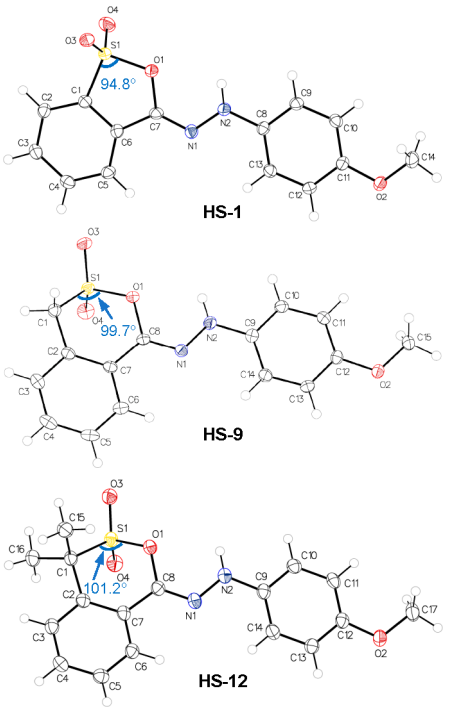

Figure 3. Crystal structures of **HS-1**, **-9**, and **-12**. The structural diagrams containing anisotropic displacement ellipsoids are drawn at the 50% probability level.

O1 angles in **HS-1**, **-9**, and **-12** are 94.8°, 99.7°, and 101.2°, respectively, indicating a gradual decrease in angle strain. Moreover, the *gem*-dimethyl group twists the SO_2 group out of the sultone ring plane, as indicated by a larger C7−C8−O1−S1 dihedral angle of 46.5° in **HS-12**, compared to 41.3° in **HS-9**. Indeed, the *gem*-dimethyl group was known to increase the sultone ring closure rate,[30] underpinning the remarkable stability of **HS-12**.

To understand the ring−chain tautomerism leading to the generation of the NI, we performed DFT calculations with **HS-1** using the SMD implicit solvation model in water. We considered two possible tautomerization pathways: a neutral one involving direct proton transfer from N to O followed by the sultone ring rupture, and an anionic one involving deprotonation of **A** to produce the anionic intermediate **B** followed by ionization to generate tautomer **C** (Figure 4a). Only the anionic tautomerization pathway was found to be energetically favorable (Figure S4), suggesting pH dependency of this process. Consequently, the calculated reaction energy diagram revealed that the cycloaddition reaction is the rate-determining step and highly exergonic, comparable to what we reported recently.[11] The HS → NI tautomerization is thermodynamically favorable (ΔG = −7.1 kcal/mol) and the barrier is surprisingly low ($\Delta G^{\ddagger}$ = 6.3 kcal/mol), suggesting the ring−chain tautomerization is spontaneous at room temperature after deprotonation. Extending this calculation to **HS-12/13** revealed that compared to **HS-1**, anionic **HS-12/13** are present in water at lower concentrations and encounter higher activation barriers in the cycloaddition reaction with BCN (Table S7).

Our computational results suggest that the position of the HS → NI tautomerization equilibrium is controlled by both pH and solvent polarity as they affect the deprotonation and ionization steps, respectively (Figure 4). To probe the pH

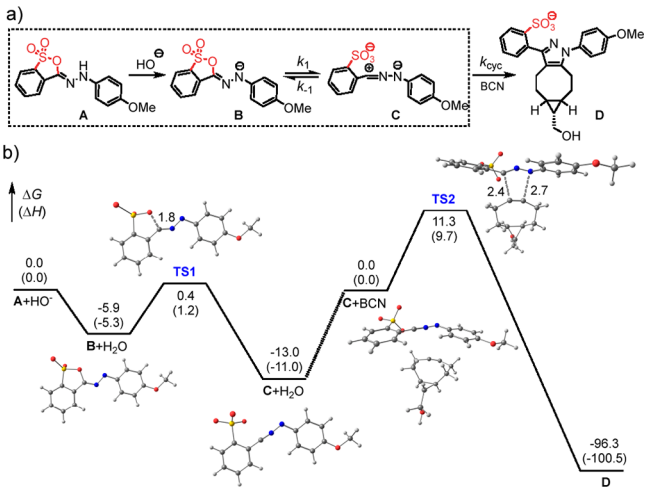

Figure 4. (a) Scheme of the reaction steps involved in HS → NI tautomerization (box) and subsequent 1,3-dipolar cycloaddition. (b) Reaction diagram showing the free energy profile involving **HS-1** and the optimized structures. **A**, neutral sultone form; **B**, anionic form of **A**; **TS1**, transition state for sultone ring rupture; **C**, nitrile imine form; **C**+BCN, reactant complex between **C** and BCN; **TS2**, transition state for the cycloaddition; **D**, cycloadduct. Energies are reported in kcal/mol, while interatomic distances at the transition states are reported in Å.

effect, we incubated **HS-1** with acetonitrile−phosphate buffer (1:1) at varying pH and observed progressive decreases in $t_{1/2}$ and concurrent increases in k_2 as pH increases from 4 to 10 (Figure S5). To probe the solvent polarity effect, we incubated **HS-14**, a water-soluble analog of **HS-13** displaying balanced stability and reactivity, with BCN in varying acetonitrile−PBS mixtures. We observed that $t_{1/2}$ remained longer than 48 h in 50−70% PBS but dropped to 139 min in 100% PBS. Concurrent increases in cycloaddition reactivity were observed; the k_2 values increased from 0.291 M^{-1} s^{-1} in 50% PBS to 40.1 M^{-1} s^{-1} in 100% PBS, a rise of 138-fold (Figure S6).

We surmised that the pH and solvent polarity control the amount of the reactive NI tautomer in the equilibria. We attempted to use ^{1}H NMR to quantify reactive NI tautomer in **HS-7** without success (Figure S7), suggesting that the NI concentration is very low. We then proceeded to calculate the fraction of reactive NI tautomer, f_{NI}, by comparing the apparent second-order rate constant of HS-mediated cycloaddition, k_2, to that of a matching tetrazole-mediated cycloaddition, k_2', using the equation $f_{NI} = k_2/k_2'$, assuming (1) the reactive NI tautomer reaches a steady state and (2) the reactivity of unprotected NI in eq 1 is identical to that of the

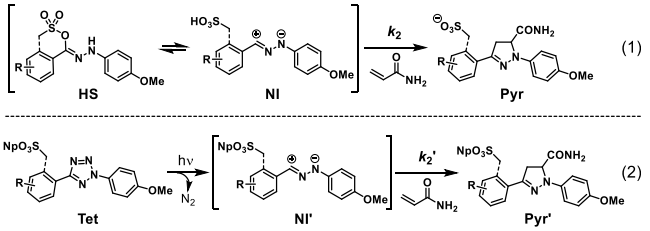

photogenerated, neopentyl (Np)-protected NI in eq 2. Using this method, we calculated f_{NI} to be 8.0 ± 0.9 × 10^{-3} for **HS-1** (Figure S8) and 1.5 ± 0.1 × 10^{-5} for **HS-13** (Figure S9). The small f_{NI} value for **HS-13** (>500-fold lower than **HS-1**)

https://doi.org/10.1021/jacs.2c12325
J. Am. Chem. Soc. 2023, 145, 9959−9964

indicates that **HS-13** mostly stays in the stable sultone form, underpinning its extraordinary stability (Table 1).

To assess the reactivity and orthogonality of HS in protein systems, we incubated a panel of NB1 nanobody[31] mutants encoding BCN-lysine (BCNK) at position-4 next to the highly variable CDR loops through genetic code expansion with **HS-14** in PBS and monitored the reactions by QTOF-LC/MS (Figures S10–S13). Interestingly, the NB1-V4BCNK mutant which contains two proximal Tyr residues reacted 8 times faster than BCN–**HS-14** ligation in solution (k_2 = 325 ± 17 M^{-1} s^{-1} vs 40.1 M^{-1} s^{-1}; Figure 5a). The reactions slowed down when either Tyr was replaced with Asp/Glu; e.g., NB1-V4BCNK-Y34D reacted at about the same rate as BCN in solution (Figure 5a; Figure S13), suggesting that rate acceleration depends critically on the Tyr residues in the BCN microenvironment. One possibility is that this microenvironment helps to shift the tautomerization equilibrium toward the reactive NI form. Importantly, no double modifications of nanobodies were detected, confirming that HS–BCN ligation is orthogonal to the proteinogenic groups.

To investigate if HS are suitable for bioorthogonal labeling in live cells, we treated HEK293T cells transiently expressing a transmembrane glucagon receptor containing a C-terminal GFP (GCGR-GFP) and a BCNK at position-372 at the extracellular loop 3 with a Cy5-conjugated **HS-13** (HS-Cy5) for 1 h. After washing, we observed that the cells expressing GCGR-H372BCNK-GFP showed strong fluorescence in Cy5 channel in confocal microscopy (Figure 5b; Figure S14). Because HS-Cy5 is cell-impermeable, the overlay image and line profile analysis confirmed the highly specific Cy5-labeling of the membrane-localized GCGR but not the endosome-localized receptors (Figure 5b).

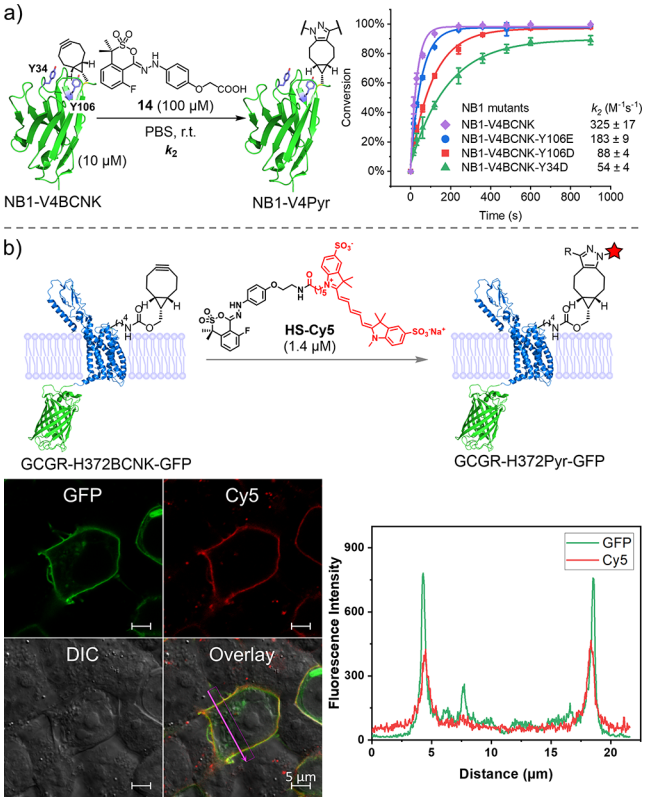

Figure 5. (a) Bioorthogonal modification of BCNK-encoded nanobodies via HS–BCN ligation. The proximal CDR1-Y34 and CDR3-Y106 are shown in purple sticks on the nanobody ribbon model (PDB code 3OGO). (b) Bioorthogonal fluorescent labeling of GCGR in live cells via HS-BCN ligation. Top: labeling scheme. Bottom left: Confocal micrographs of HEK 293T cells expressing GCGR-H372BCNK-GFP after 1 h incubation in DMEM medium containing 1.4 μM HS-Cy5. Bottom right: Line profile analysis of the overlaid image on the left showing specific membrane receptor labeling.

In summary, we have developed a new class of bioorthogonal reagents called hydrazonyl sultones (HS) that serve as stable tautomers of highly reactive nitrile imines (NI). HS displayed a broad range of aqueous stability and tunable reactivity in a 1,3-dipolar cycloaddition reaction depending on substituents, sultone ring structure, and solvent conditions. A water-soluble HS showed an optimal combination of stability ($t_{1/2}$ = 139 min) and reactivity (k_2 = 40.1 M^{-1} s^{-1}) in PBS. DFT calculations offered vital insights into the HS → NI tautomerism. Comparative kinetic analysis revealed that a tiny fraction of reactive NI (~15 ppm) is present in the tautomeric mixture, underpinning the extraordinary stability observed for the six-membered HS. The bioorthogonal reactivity of HS was demonstrated through fast and selective modification of the BCNK-encoded nanobodies in PBS with k_2 values as high as 325 M^{-1} s^{-1}. Furthermore, a Cy5-conjugated HS enabled robust and selective fluorescent labeling of GCGR encoding BCNK at the extracellular loop 3 on live cells. Since a BCN-encoded nanobody library can be generated by varying the residues at the CDR loops and screened for enhanced reactivity, we envision that a highly reactive nanobody-based reactant module can be rapidly evolved in the future. Combined with a recognition module, the HS–BCN ligation could be useful in the design of nanobody-based probes for pretargeted PET imaging in living animals.[32]

■ ASSOCIATED CONTENT

Supporting Information

The Supporting Information is available free of charge at https://pubs.acs.org/doi/10.1021/jacs.2c12325.

Supplemental figures and tables, synthetic schemes, experimental procedures, computational details, and characterization of all new compounds (PDF)

Accession Codes

CCDC 2218134–2218136 contain the supplementary crystallographic data for this paper. These data can be obtained free of charge via www.ccdc.cam.ac.uk/data_request/cif, or by emailing data_request@ccdc.cam.ac.uk, or by contacting The Cambridge Crystallographic Data Centre, 12 Union Road, Cambridge CB2 1EZ, UK; fax: +44 1223 336033.

■ AUTHOR INFORMATION

Corresponding Author

Qing Lin – *Department of Chemistry, State University of New York at Buffalo, Buffalo, New York 14260-3000, United States;* orcid.org/0000-0002-9196-5718; Email: qinglin@buffalo.edu

Authors

Ming Fang – *Department of Chemistry, State University of New York at Buffalo, Buffalo, New York 14260-3000, United States;* orcid.org/0000-0002-1566-4825

Gangam Srikanth Kumar – *Department of Chemistry, State University of New York at Buffalo, Buffalo, New York*

14260-3000, United States; orcid.org/0000-0002-6052-9913

Stefano Racioppi − *Department of Chemistry, State University of New York at Buffalo, Buffalo, New York 14260-3000, United States;* orcid.org/0000-0002-4174-1732

Heyang Zhang − *Department of Chemistry, State University of New York at Buffalo, Buffalo, New York 14260-3000, United States*

Johnathan D. Rabb − *Department of Chemistry, State University of New York at Buffalo, Buffalo, New York 14260-3000, United States*

Eva Zurek − *Department of Chemistry, State University of New York at Buffalo, Buffalo, New York 14260-3000, United States;* orcid.org/0000-0003-0738-867X

Complete contact information is available at: https://pubs.acs.org/10.1021/jacs.2c12325

Notes

The authors declare no competing financial interest.

■ ACKNOWLEDGMENTS

We gratefully acknowledge the National Institutes of Health (Grant R35GM130307 to Q.L.) for financial support. We thank Alan Siegel at SUNY Buffalo Biological Sciences Imaging Facility for assistance with confocal microscopy and Zheng Wang for assistance with nanobody mutant expression and purification. The crystal structures of HS-1, -9, and -12 have been deposited into Cambridge Crystallographic Data Centre with deposit numbers CCDC 2218134, 2218136, and 2218135, respectively. Computations were carried out at the Center for Computational Research at SUNY Buffalo, partly supported by the National Science Foundation (Grant OAC-1724891) and the National Institutes of Health (Grant S10OD024973).

■ REFERENCES

(1) Sletten, E. M.; Bertozzi, C. R. Bioorthogonal Chemistry: Fishing for Selectivity in a Sea of Functionality. *Angew. Chem. Int. Ed* **2009**, *48*, 6974.

(2) Devaraj, N. K. The Future of Bioorthogonal Chemistry. *ACS Cent Sci.* **2018**, *4*, 952−959.

(3) Scinto, S. L.; Bilodeau, D. A.; Hincapie, R.; Lee, W.; Nguyen, S. S.; Xu, M.; am Ende, C. W.; Finn, M. G.; Lang, K.; Lin, Q.; Pezacki, J. P.; Prescher, J. A.; Robillard, M. S.; Fox, J. M. Bioorthogonal chemistry. *Nat. Rev. Methods Primers* **2021**, *1*, 30.

(4) Kumar, G. S.; Lin, Q. Seeking Citius: Photochemical Access of Reactive Intermediates for Faster Bioorthogonal Reactions. *ChemBioChem* **2022**, *23*, e202200175.

(5) Kumar, G. S.; Lin, Q. Light-Triggered Click Chemistry. *Chem. Rev.* **2021**, *121*, 6991−7031.

(6) Albada, B.; Keijzer, J. F.; Zuilhof, H.; van Delft, F. Oxidation-Induced "One-Pot" Click Chemistry. *Chem. Rev.* **2021**, *121*, 7032−7058.

(7) Liu, L.; Zhang, D.; Johnson, M.; Devaraj, N. K. Light-activated tetrazines enable precision live-cell bioorthogonal chemistry. *Nat. Chem.* **2022**, *14*, 1078−1085.

(8) Li, J.; Kong, H.; Huang, L.; Cheng, B.; Qin, K.; Zheng, M.; Yan, Z.; Zhang, Y. Visible Light-Initiated Bioorthogonal Photoclick Cycloaddition. *J. Am. Chem. Soc.* **2018**, *140*, 14542−14546.

(9) Lim, R. K. V.; Lin, Q. Azirine ligation: fast and selective protein conjugation via photoinduced azirine-alkene cycloaddition. *Chem. Commun.* **2010**, *46*, 7993−7995.

(10) Zhang, L.; Zhang, X.; Yao, Z.; Jiang, S.; Deng, J.; Li, B.; Yu, Z. Discovery of Fluorogenic Diarylsydnone-Alkene Photoligation: Conversion of ortho-Dual-Twisted Diarylsydnones into Planar Pyrazolines. *J. Am. Chem. Soc.* **2018**, *140*, 7390−7394.

(11) Kumar, G. S.; Racioppi, S.; Zurek, E.; Lin, Q. Superfast Tetrazole-BCN Cycloaddition Reaction for Bioorthogonal Protein Labeling on Live Cells. *J. Am. Chem. Soc.* **2022**, *144*, 57−62.

(12) Jemas, A.; Xie, Y.; Pigga, J. E.; Caplan, J. L.; Am Ende, C. W.; Fox, J. M. Catalytic Activation of Bioorthogonal Chemistry with Light (CABL) Enables Rapid, Spatiotemporally Controlled Labeling and No-Wash, Subcellular 3D-Patterning in Live Cells Using Long Wavelength Light. *J. Am. Chem. Soc.* **2022**, *144*, 1647−1662.

(13) Zhang, H.; Trout, W. S.; Liu, S.; Andrade, G. A.; Hudson, D. A.; Scinto, S. L.; Dicker, K. T.; Li, Y.; Lazouski, N.; Rosenthal, J.; Thorpe, C.; Jia, X.; Fox, J. M. Rapid Bioorthogonal Chemistry Turn-on through Enzymatic or Long Wavelength Photocatalytic Activation of Tetrazine Ligation. *J. Am. Chem. Soc.* **2016**, *138*, 5978−5983.

(14) Wang, C.; Zhang, H.; Zhang, T.; Zou, X.; Wang, H.; Rosenberger, J. E.; Vannam, R.; Trout, W. S.; Grimm, J. B.; Lavis, L. D.; Thorpe, C.; Jia, X.; Li, Z.; Fox, J. M. Enabling In Vivo Photocatalytic Activation of Rapid Bioorthogonal Chemistry by Repurposing Silicon-Rhodamine Fluorophores as Cytocompatible Far-Red Photocatalysts. *J. Am. Chem. Soc.* **2021**, *143*, 10793−10803.

(15) Borrmann, A.; Fatunsin, O.; Dommerholt, J.; Jonker, A. M.; Löwik, D. W. P. M.; van Hest, J. C. M.; van Delft, F. L. Strain-Promoted Oxidation-Controlled Cyclooctyne−1,2-Quinone Cycloaddition (SPOCQ) for Fast and Activatable Protein Conjugation. *Bioconjugate Chem.* **2015**, *26*, 257−261.

(16) Bruins, J. J.; Westphal, A. H.; Albada, B.; Wagner, K.; Bartels, L.; Spits, H.; van Berkel, W. J. H.; van Delft, F. L. Inducible, Site-Specific Protein Labeling by Tyrosine Oxidation−Strain-Promoted (4 + 2) Cycloaddition. *Bioconjugate Chem.* **2017**, *28*, 1189−1193.

(17) Yu, Z.; Ohulchanskyy, T. Y.; An, P.; Prasad, P. N.; Lin, Q. Fluorogenic, two-photon-triggered photoclick chemistry in live mammalian cells. *J. Am. Chem. Soc.* **2013**, *135*, 16766−16769.

(18) Lederhose, P.; Chen, Z.; Müller, R.; Blinco, J. P.; Wu, S.; Barner-Kowollik, C. Near-Infrared Photoinduced Coupling Reactions Assisted by Upconversion Nanoparticles. *Angew. Chem. Int. Ed* **2016**, *55*, 12195−12199.

(19) Jones, P. R. Ring-Chain Tautomerism. *Chem. Rev.* **1963**, *63*, 461−487.

(20) Dory, Y. L.; Roy, A.-L.; Soucy, P.; Deslongchamps, P. Study of Very Reactive Tautomeric Phenol Dienones as Dienes in Diels−Alder Reactions. *Org. Lett.* **2009**, *11*, 1197−1200.

(21) Xi, Z.; Kong, H.; Chen, Y.; Deng, J.; Xu, W.; Liang, Y.; Zhang, Y. Metal- and Strain-Free Bioorthogonal Cycloaddition of o-Diones with Furan-2(3H)-one as Anionic Cycloaddend. *Angew. Chem., Int. Ed* **2022**, *61*, e202200239.

(22) An, P.; Lewandowski, T. M.; Erbay, T. G.; Liu, P.; Lin, Q. Sterically Shielded, Stabilized Nitrile Imine for Rapid Bioorthogonal Protein Labeling in Live Cells. *J. Am. Chem. Soc.* **2018**, *140*, 4860−4868.

(23) Uno, S.-n.; Kamiya, M.; Yoshihara, T.; Sugawara, K.; Okabe, K.; Tarhan, M. C.; Fujita, H.; Funatsu, T.; Okada, Y.; Tobita, S.; Urano, Y. A spontaneously blinking fluorophore based on intramolecular spirocyclization for live-cell super-resolution imaging. *Nat. Chem.* **2014**, *6*, 681−689.

(24) Wang, L.; Tran, M.; D'Este, E.; Roberti, J.; Koch, B.; Xue, L.; Johnsson, K. A general strategy to develop cell permeable and fluorogenic probes for multicolour nanoscopy. *Nat. Chem.* **2020**, *12*, 165−172.

(25) Hansch, C.; Leo, A.; Taft, R. W. A Survey of Hammett Substituent Constants and Resonance and Field Parameters. *Chem. Rev.* **1991**, *91*, 165−195.

(26) Lee, J. W.; Lee, K. N.; Ngai, M.-Y. Synthesis of Tri- and Difluoromethoxylated Compounds by Visible-Light Photoredox Catalysis. *Angew. Chem. Int. Ed* **2019**, *58*, 11171−11181.

(27) Jiang, S.; Wu, X.; Liu, H.; Deng, J.; Zhang, X.; Yao, Z.; Zheng, Y.; Li, B.; Yu, Z. Ring-Strain-Promoted Ultrafast Diaryltetrazole−Alkyne Photoclick Reactions Triggered by Visible Light. *ChemPhotoChem* **2020**, *4*, 327−331.

(28) Bordwell, F. G.; Osborne, C. E.; Chapman, R. D. The Hydrolysis of Sultones - the Effect of Methyl Groups on the Rates of Ring-Opening Solvolyses. *J. Am. Chem. Soc.* **1959**, *81*, 2698−2705.
(29) Wang, Y.; Song, W.; Hu, W. J.; Lin, Q. Fast Alkene Functionalization In Vivo by Photoclick Chemistry: HOMO Lifting of Nitrile Imine Dipoles. *Angew. Chem. Int. Ed* **2009**, *48*, 5330−5333.
(30) Jager, J.; Graafland, T.; Schenk, H.; Kirby, A. J.; Engberts, J. B. F. N. Intramolecular-Catalyzed Sulfonamide Hydrolysis. 7. The Thorpe-Ingold Effect in the Intramolecular Carboxyl-Catalyzed Hydrolysis of Sulfonamides. *J. Am. Chem. Soc.* **1984**, *106*, 139−143.
(31) Kubala, M. H.; Kovtun, O.; Alexandrov, K.; Collins, B. M. Structural and thermodynamic analysis of the GFP:GFP-nanobody complex. *Protein Sci.* **2010**, *19*, 2389−2401.
(32) Meyer, J.-P.; Houghton, J. L.; Kozlowski, P.; Abdel-Atti, D.; Reiner, T.; Pillarsetty, N. V. K.; Scholz, W. W.; Zeglis, B. M.; Lewis, J. S. 18F-Based Pretargeted PET Imaging Based on Bioorthogonal Diels−Alder Click Chemistry. *Bioconjugate Chem.* **2016**, *27*, 298−301.

https://doi.org/10.1021/jacs.2c12325
J. Am. Chem. Soc. 2023, 145, 9959−9964